THE HURRICANE IMAGING RADIOMETER WIDE SWATH SIMULATION AND WIND SPEED RETRIEVALS

Ruba A. Amarin[1], Linwood Jones[1], James Johnson[1], Chris Ruf[2], Timothy L. Miller[3] and Eric Uhlhorn[4]

[1] Central Florida Remote Sensing Laboratory
University of Central Florida, Orlando, Florida 32816, U.S.A
* ramarin@mail.ucf.edu
[2] Space Physics Research Laboratory, University of Michigan, Ann Arbor, Michigan
[3] NASA Marshall Space Flight Center, Huntsville, Alabama
[4] NOAA/AOML/Hurricane Research Division, Miami, Florida, USA

ABSTRACT

The knowledge of peak winds in hurricanes is critical to classification of hurricane intensity; therefore, there is a strong interest in the operational remote sensing of ocean surface winds for monitoring tropical storms and hurricanes, especially those which threaten landfall. Presently, the airborne Stepped Frequency Microwave Radiometer (SFMR) is the state-of-the-art remote sensor for providing this information in real-time, during hurricane surveillance flights. However, for the future, NASA and NOAA are collaborating in the development of the Hurricane Imaging Radiometer (HIRAD), which is a prototype of the next-generation high-flying airborne instrument for monitoring hurricanes.

This paper describes a realistic end-to-end simulation of HIRAD hurricane measurements while flying on an unmanned Global Hawk aircraft. The objective of this research is to develop baseline retrieval algorithms and provide a wind speed measurement accuracy assessment for the upcoming NASA hurricane field program, Genesis and Rapid Intensification Processes (GRIP), to be conducted in 2010.

Index Terms— HIRAD, hurricane imaging, microwave radiometry, wind speed retrievals

1. HIRAD TECHNOLOGY

The HIRAD aircraft instrument was developed over the past 4 years under a NASA Marshall Space Flight Center led collaboration with NOAA's Atlantic Oceanographic and Meteorological Laboratory, Hurricane Research Division, the Central Florida Remote Sensing Laboratory (CFRSL) at the University of Central Florida and the Space Physics Research Laboratory of the University of Michigan. This is new technology that offers significant new capability for hurricane research and future operational surveillance.

HIRAD is a synthetic aperture interferometric microwave radiometer [1, 2] that operates at four C-band frequencies (4, 5, 6 & 6.6 GHz) that is based on the successful Stepped Frequency Microwave Radiometer, SFMR, routinely used by NOAA in hurricane surveillance [3]. HIRAD uses a microstrip thinned array antenna to synthesize cross-track pushbroom images of ocean surface wind speed and rain rate, which enables wide swath imaging of the hurricane compared to the nadir viewing ground track profiles of SFMR. From a 20 km altitude, the HIRAD design produces a worst-case spatial resolution at nadir of 2.5 km at 4 GHz and a cross-track measurement swath of 60 km (± 60° field-of-view). HIRAD will potentially succeed SFMR as the primary source of surface wind data in NOAA's hurricane surveillance program, and this instrument is a prototype for the future development of a sub-orbital (high flying unmanned aircraft) and space-based satellite hurricane surveillance system. In this paper, results are presented for an end-to-end simulation of HIRAD with 41 equivalent antenna beams (with boresight spaced on 3° centers ±60°).

2. END-TO-END SIMULATION

A simplified block diagram to the HIRAD end-to-end simulation is shown in Fig. 1. The first step is performing the geometry module calculations, where the HIRAD pushbroom antenna beams lines-of-sight and surface footprints are calculated. As part of the forward radiative transfer model (RTM), several numerical hurricane model runs are used that provide realistic 3D environmental parameters (rain, water vapor, clouds, temperature and surface winds) from which simulated HIRAD T_b's are derived for typical flight tracks from platforms operating at 20 km altitude. The RTM includes the SFMR rain model for the hurricane environment and an ocean surface emissivity model developed especially for HIRAD high incidence angle measurements [5]. A detailed description is provided later in this section. Also included in the simulation is antenna pattern convolution of the scene T_b.

In the HIRAD retrieval algorithm, a different RTM is used with environmental parameters available from independent climatology and data bases parametrically to compute a theoretical modeled brightness temperature matrix over a wide range of possible wind speed, rain rate and incidence angles for the four HIRAD frequencies.

The retrieved ocean surface wind speed and rain rate are estimated using the statistical least-squares difference method. In this procedure, the wind speed and rain rate that minimize the difference between the simulated HIRAD T_b measurements and modeled apparent brightness temperatures across all HIRAD frequencies. Realistic sources of random errors, which are expected in hurricane observations, are added to the simulated HIRAD measurements and the retrievals are performed using a Monte Carlo simulation. The retrieval algorithm is performed using independent available databases of sea surface temperatures and climatological hurricane atmospheric parameters (excluding

rain) as a priori information. The retrieval algorithm process is described in the bottom part of Fig. 1, and a detailed description of the retrieval algorithm process is provided in section 4 of this paper.

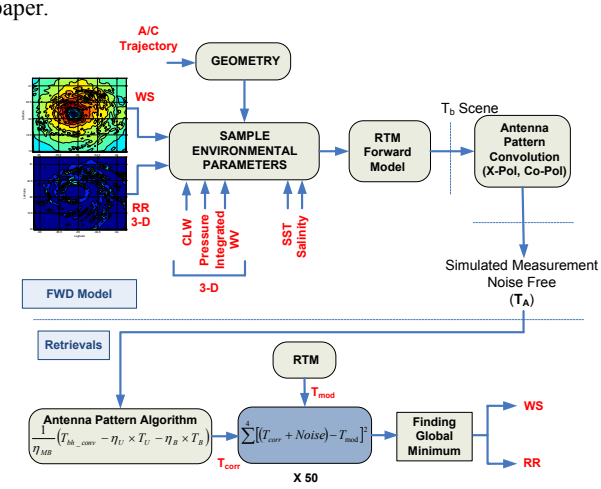

Figure 1 HIRAD end-to-end simulation.

2.1. Forward Radiative Transfer Model

Significant advances in radiative transfer modeling (RTM) of hurricanes have been developed at CFRSL to simulate HIRAD radiometric brightness temperature (T_b) scenes. Specifically, an improved ocean surface emissivity model that extends to large incidence angles (> 60°) and high wind speeds (> 70 m/sec), has been developed [6]. Further, the RTM includes the SFMR rain model for the hurricane environment, which is from the work of Jorgensen and Willis [4] and Olsen et al. [5].

Two hurricane "nature run" simulations were used in this paper; the Penn State–NCAR fifth-generation Mesoscale Model (MM5) described by Chen et al. (2007) [7] and the Weather Research and Forecasting (WRF) model used by NOAA, HRD. The two model runs for Hurricane Frances (MM5, 2004) and Hurricane Bill (WRF, 2009) provide realistic 3D environmental parameters of rain, water vapor, clouds and surface winds from which simulated HIRAD T_b's are derived for typical aircraft "Fig-4" flight pattern as shown in Fig. 2.

The RTM is used to compute the absorption coefficients for water vapor, cloud liquid water, rain and oxygen. For environmental parameters, we use 3D fields produced by the simulated nature run and a realistic high-resolution sea surface temperature (SST) field from the NSSTC. Each simulated HIRAD T_b measurement (cross-track pixel) has a unique surface wind speed and line-of-sight atmospheric profile, which uses a mesh grid of 39 atmospheric layers and the horizontal grid of 1.67 km pixels. This procedure calculates the simulated HIRAD pushbroom geometry based on the HIRAD antenna sampling for the cross-track scans.

2.2. Antenna Pattern Convolution

The HIRAD measurement is H-Pol only, but to simulate realistic antenna temperature measurements, both the H-Pol and V-Pol scene apparent T_b are computed from the forward model and are convolved with the co-polarized (Co-Pol) and cross-polarized (X-Pol) antenna patterns respectively. The resulted convolved H-Pol and V-Pol temperatures are given by [8],

$$T_{bH_{conv}} = \frac{\int_0^{2\pi}\int_{-\theta 1}^{\theta 1} T_{ap\,h}(\theta,\phi)\times F_{Co-Pol}(\theta,\phi)\times sin\theta d\,\theta d\phi}{\int_0^{2\pi}\int_{-\theta}^{\theta} F_{Co-Pol}(\theta,\phi)\times sin\theta d\,\theta d\phi} \quad (1)$$

$$T_{bV_{conv}} = \frac{\int_0^{2\pi}\int_{-\theta}^{\theta} T_{apv}(\theta,\phi)\times F_{X-Pol}(\theta,\phi)\times sin\theta d\,\theta d\phi}{\int_0^{2\pi}\int_{-\theta}^{\theta} F_{X-Pol}(\theta,\phi)\times sin\theta d\,\theta d\phi} \quad (2)$$

The final convolved brightness temperature, T_A, is a superposition of T_{bHconv} and T_{bVconv} according to,

$$T_A = (1-\gamma)T_{bH_{conv}} + \gamma T_{bV_{conv}} \quad (3)$$

where γ is the ratio of the X-Pol brightness temperature to the total, which increases (degrades) with incidence angle and is approximated by,

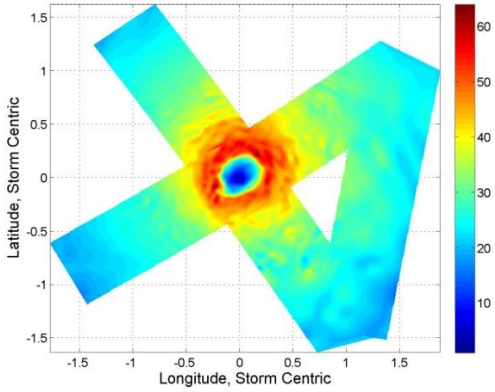

Figure 2 Example of simulated HIRAD wind speed image for Hurricane Frances with color bar in m/s. Aircraft Fig-4 flight lines from an altitude of 20 km.

$$\gamma = \frac{\int_{\text{First Nulls}} F_{X-Pol}(\theta,\phi)\times\sin(\theta)d\theta}{\int_{\text{First Nulls}} F_{X-Pol}(\theta,\phi)\times\sin(\theta)d\theta + \int_{\text{First Nulls}} F_{Co-Pol}(\theta,\phi)\times\sin(\theta)d\theta} \quad (4)$$

3. WIND SPEED AND RAIN RATE RETRIEVAL ALGORITHM

The HIRAD algorithm, for rain rate and wind speed retrievals in hurricanes, is composed of a retrieval RTM and an inversion algorithm as described earlier by Fig. 1 (bottom part).

3.1. Atmospheric Treatment

The retrieval RTM is different than the forward RTM used in the T_b measurement simulation. For the retrieval, an a priori hurricane climatology atmosphere profile, based upon radial distance from the hurricane eye, is used at each surface beam position. Azimuthally averaged water vapor and cloud liquid water vertical profiles were constructed over radial annuli of 5 km thicknesses using the nature run data.

Because rain is a retrieved parameter, it is treated differently in the retrieval RTM. Here the rain is assumed to be uniform along the slant path from the assumed constant freezing level of 5 km to the surface. Also for the retrieval RTM, the SST is assumed to be a constant value of 28 Celsius in comparison to the actual SST image used in the forward RTM T_b simulation. The sum of these

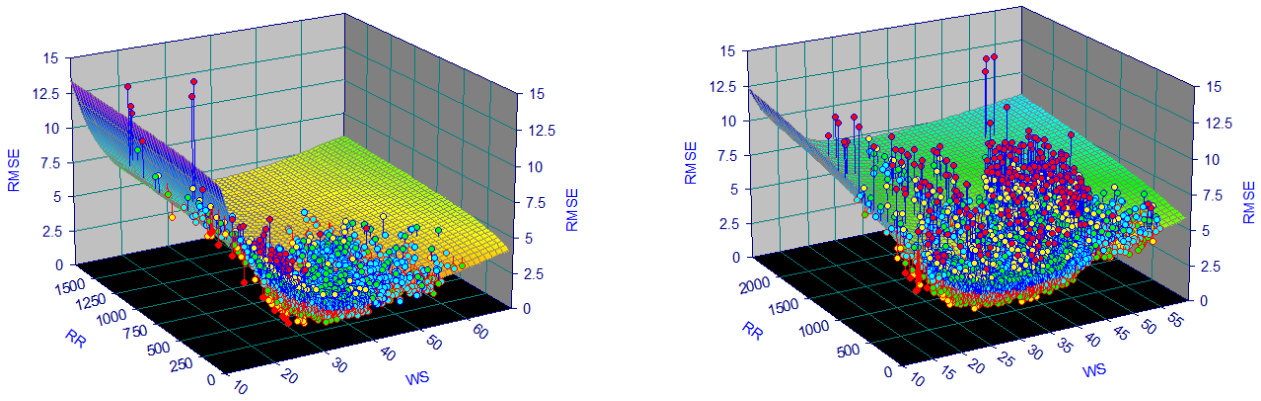

(a) (b)

Figure 3 RMS retrieved wind speed error surfaces (m/s) for (a) Nadir and (b) ± 60° for 4 K random error.

absorption coefficients along with the absorption coefficient due to rain (retrieved parameter) is used in the computation of the modeled brightness temperature (T_{mod}) at each of the four C-band frequencies.

3.2. Antenna Pattern Correction

It is necessary to correct for the antenna pattern convolution effect and thereby estimate the true boresight brightness temperature before performing the wind speed and rain rate retrieval. The cross-pol (V-Pol) effect was removed from the total antenna brightness temperature (T_A) computation according to,

$$T_{bH_{conv}} = \frac{T_A - \gamma \times T_{bV\_conv}}{(1-\gamma)} \quad (5)$$

The V-Pol convolved temperatures, T_{bV_conv}, in (5) are estimated based on empirical correations of the convolved antenna brightness temperature, T_A, using the simulated forward model T_b's for the two nature runs. After solving for T_{bHconv}, the estimated boresight brightness temperature, T_{corr}, is given in (6),

$$T_{Corr} = \frac{1}{\eta_{ML}}\left[T_{bH_{conv}} - \eta_U \times T_U - \eta_B \times T_B\right] \quad (6)$$

where T_U and T_B are the brightness temperatures that correspond to the "above the boresight" and "below the boresight" portions of the pattern. These T_b's are computed as part of the simulated forward model based on the observed regressions with T_A. , and η_{ML}, η_U, and η_B are the correspondent beam efficiencies of the main lobe, above and below the boresight respectively.

Also included in the retrieval algorithm are realistic sources of errors which are expected in hurricane observations and include the instrument T_b errors which involves the NEDT and the ΔG/G, the aircraft attitude and the geophysical model function (emissivity model) errors. In the simplest terms, these T_b errors are modeled as random errors that have probability distribution functions that are Gaussian random distributions with standard deviations that vary parametrically from 1 to 8 Kelvin.

The modeled brightness temperature matrix, T_{mod}, is compared to the corrected brightness temperature with random errors added, (T_{corr} + *Noise*), at each of the four frequencies. Each element in the difference matrices is squared and the algorithm searches for the local minimum of the summed squared difference surface, over all frequencies. This process is repeated 50 times in a Monte-Carlo simulation for each beam position and scan to collect RMSE statistics.

4. RESULTS

This section includes results from a Monte Carlo simulation of HIRAD T_b's, with errors, and retrieved wind speed and rain rate. A single Fig-4 flight pattern, with 2 perpendicular flight legs through the eye of a hurricane 90° apart would adequately cover the inner portion of the hurricane and measure the maximum winds. However, to build a larger data set for this error analysis, six Fig-4 patterns were simulated, with 12 flight legs 30° apart. Each flight leg is made up of 240 individual HIRAD scans, resulting in a total of 3840 scans over the HIRAD swath. The simulated HIRAD swath consists of 41 cross-track pixels of T_b, and the Monte Carlo simulation adds zero-mean Gaussian random errors. The nature run modeled data, serving as surface truth, is compared to the retrieved wind speed values and rain rate values and RMS errors are computed from the differences.

To characterize the wind speed retrieval error as a function of wind speed, rain rate and beam position (EIA), a regression analysis was performed to fit wind speed "error surfaces" in two dimensions (wind speed and integrated rain rate) for fixed incidence angles. The errors were the RMS of the Monte Carlo retrieval simulation on a per pixel basis for all cross-track scans.

Example results presented in Fig. 3 were computed for all Fig-4 legs, and a 4 K random error, which shows the best wind speed RMSE surface fits (based on maximizing "Coefficient of Determination") at Nadir and 60° beam positions. Each symbol represents an individual (pixel) estimate of the wind speed error. The magnitude of the wind speed error increases with increasing EIA, but the shape of the surface i.e., the dependence of the error on wind speed and rain rate is similar at all EIAs. The RMS wind speed errors, at all beam positions, are the greatest at lower wind speeds, and in general the error increases with rain rate.

Taking constant wind speed slices of these surfaces is a useful way to look at this data, so RMSE is plotted against integrated rain rate for constant wind speeds at Nadir and ± 60° in Fig. 4.

5. SUMMARY

The Hurricane Imaging Radiometer, HIRAD, instrument concept has the potential to improve on the state of the art for hurricane surface wind speed measurements currently provided by SFMR. This improved capability to provide a wide swath measurement

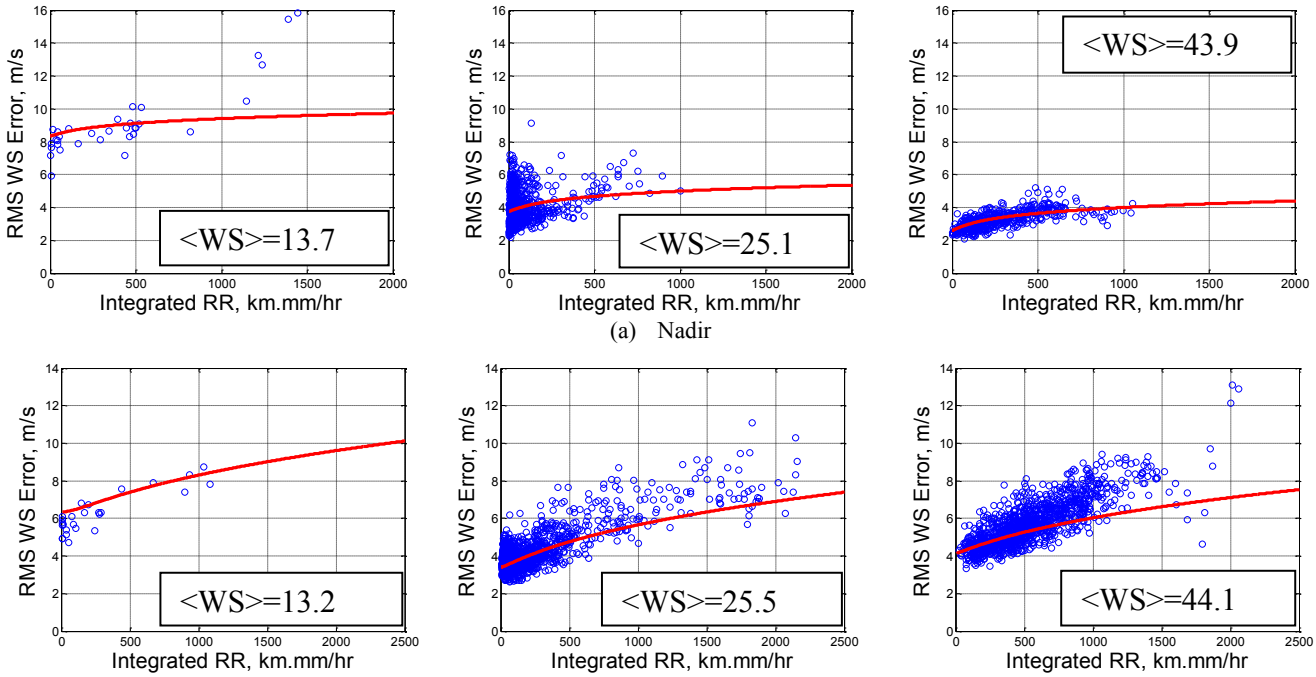

(a) Nadir

(b) ± 60 degrees

Figure 4 RMS wind speed errors (m/s) at (a) Nadir, (b) ± 60° for three wind speed bins for 4 K random error.

compared to the SFMR nadir viewing profile of brightness temperature has very significant positive impact on hurricane surveillance. The HIRAD simulation is composed of a forward radiative transfer model, to calculate realistic brightness temperature measurements in a 3D treatment of the atmospheric components and rain, and a statistical least-squares difference inversion algorithm which was based on the HIRAD geometry and the basic HIRAD antenna design. Nature, or surface truth, was represented by the MM5 and WRF numerical models for wind and rain fields for hurricane Frances, 2004, and hurricane Bill, 2009 respectively.

Monte Carlo error studies were conducted for simulated HIRAD surveillance flights in hurricanes Frances and Bill. Sixteen flight lines were simulated to provide complete images of Frances with brightness temperature errors of 1, 2, 4, and 8 Kelvin applied. The modeled surface truth and the simulated retrievals were compared and the resulting differences, or root mean squared errors, RMSE for wind speed in the presence of rain were computed. It was observed that the retrieved wind speed compares well to the surface truth over most of the swath. Antenna pattern effects and limitations to the treatment of rain in the retrieval algorithm did result in some significant wind speed errors, usually near the edges of the swath (± 60°). The wind speed retrieval error was further characterized as a function of wind speed, rain rate and beam position, by computing wind speed error surfaces. These relationships showed that the magnitude of the wind speed error increases with increasing EIA, and the shape of the dependence of the error on wind speed and rain rate is similar at all EIAs. The RMS wind speed errors are the greatest at lower wind speeds, due to the shape of the surface emissivity GMF, and this is true at all beam positions.

6. REFERENCES

[1] David M. Le Vine, Andrew J. Griffis, Calvin T. Swift, and Thomas J. Jackson, 'ESTAR: A Synthetic Aperture Microwave Radiometer for Remote Sensing Applications', *Proceedings of the IEEE*, vol. 82. NO 12 December 1994.

[2] Johnson, James W., Amarin, R. A., El-Nimri, Salem F., and W. Linwood Jones "A Wide-Swath, Hurricane Imaging Radiometer for Airborne Operational Measurements", *Proc. IEEE IGARSS-06*, Aug. 28 - Sept. 1, 2006, Denver, CO.

[3] E. W. Uhlhorn, P. G. Black, J. L. Franklin, M. Goodberlet, J. Carswell, A. S. Goldstein "Hurricane Surface Wind Measurements from an Operational Stepped Frequency Microwave Radiometer," *American Meteorological Society*, 2007.

[4] D. P. Jorgensen and P. T. Willis, "A Z-R Relationship for Hurricanes," *Journal of Applied Meteorology*, vol. 21, pp. 356-366, 1982.

[5] R. L. Olsen, D. V. Rogers, and D. B. Hodge, "The aRb Relation in the Calculation of Rain Attenuation," *IEEE Trans. Antennas Propagat.*, vol. 26, pp. 318-329, 1978.

[6] Salem Fawwaz El-Nimri, W. Linwood Jones, Eric Uhlhorn, Christopher Ruf , James Johnson, and Peter Black, "An Improved C-band Ocean Surface Emissivity Model at Hurricane-force Wind Speeds over a Wide Range of Earth Incidence Angles," *IEEE Geoscience and Remote Sensing Letters, 2009.*

[7] Chen, S. S., J. F. Price, W. Zhao, M. A. Donelan, E. J. Walsh, "The CBLAST-Hurricane Program and the Next-Generation Fully Coupled Atmosphere-Wave-Ocean Models for Hurricane Research and Prediction," *Bull. Amer. Meteor. Soc.*, 88(3), 311-317, 2007.

[8] F. T. Ulaby, R. K. M. Moore, and A. K. Fung, Microwave Remote Sensing, Active and Passive vol. 1. Norwood, MA: Artech House Inc, 1981.